


## RESEARCH ARTICLE

# Quantification of left ventricular myocardial strain: Comparison between MRI tagging, MRI feature tracking, and ultrasound speckle tracking

Yentl Brandt<sup>1,2</sup> | Jolijn M. Lubrecht<sup>2,3</sup> | Bouke P. Adriaans<sup>1,2,4</sup> |  
Jean-Paul Aben<sup>5</sup> | Suzanne C. Gerretsen<sup>1</sup> | Chahinda Ghossein-Doha<sup>4</sup> |  
Marc E. A. Spaanderman<sup>6,7</sup> | Frits W. Prinzen<sup>2,3</sup> | M. Eline Kooi<sup>1,2</sup> 

<sup>1</sup>Department of Radiology and Nuclear Medicine, Maastricht University Medical Centre, Maastricht, The Netherlands

<sup>2</sup>Cardiovascular Research Institute Maastricht (CARIM), Maastricht University, Maastricht, The Netherlands

<sup>3</sup>Department of Physiology, Maastricht University, Maastricht, The Netherlands

<sup>4</sup>Department of Cardiology, Maastricht University Medical Centre, Maastricht, The Netherlands

<sup>5</sup>Department of Research and Development, Pie Medical Imaging B.V., Maastricht, The Netherlands

<sup>6</sup>Department of Obstetrics and Gynecology, Maastricht University Medical Centre, Maastricht, The Netherlands

<sup>7</sup>Department of Obstetrics and Gynecology, Radboud University Medical Centre, Nijmegen, The Netherlands

## Correspondence

M. Eline Kooi, Department of Radiology and Nuclear Medicine, Maastricht University Medical Centre (MUMC+), PO Box 5800, 6202 AZ Maastricht, The Netherlands.  
Email: [eline.kooi@mumc.nl](mailto:eline.kooi@mumc.nl)

## Funding information

This retrospective study received no additional funding.

## Abstract

Ultrasound speckle tracking is frequently used to quantify myocardial strain, and magnetic resonance imaging (MRI) feature tracking is rapidly gaining interest. Our aim is to validate cardiac MRI feature tracking by comparing it with the gold standard method (i.e., MRI tagging) in healthy subjects and patients. Furthermore, we aim to perform an indirect validation by comparing ultrasound speckle tracking with MRI feature tracking. Forty-two subjects (17 formerly preeclamptic women, three healthy women, and 22 left bundle branch block patients of both sexes) received 3-T cardiac MRI and echocardiography. Cine and tagged MRI, and B-mode ultrasound images, were acquired. Inpatient global and segmental left ventricular circumferential (MRI tagging vs. MRI feature tracking) and longitudinal (MRI feature tracking vs. ultrasound speckle tracking) peak strain and time to peak strain were compared between the three techniques. Intraclass correlation coefficient (ICC) (< 0.50 = poor, 0.50–0.75 = moderate, > 0.75–0.90 = good, > 0.90 = excellent) and Bland–Altman analysis were used to assess correlation and bias;  $p$  less than 0.05 indicates a significant ICC or bias. Global peak strain parameters showed moderate-to-good correlations between methods (ICC = 0.71–0.83,  $p < 0.01$ ) with no significant biases. Global time to peak strain parameters showed moderate-to-good correlations (ICC = 0.56–0.82,  $p < 0.01$ ) with no significant biases. Segmental peak strains showed significant biases in all parameters and moderate-to-good correlation (ICC = 0.62–0.77,  $p < 0.01$ ), except for lateral longitudinal peak strain (ICC = 0.23,  $p = 0.22$ ). Segmental time to peak strain parameters showed moderate-to-good correlation (ICC = 0.58–0.74,  $p < 0.01$ ) with no significant biases. MRI feature tracking is a valid method to examine myocardial strain, but there is bias in absolute segmental strain values

**Abbreviations:** FT, feature tracking; (G/S/L)CPS, (global/septal/lateral) circumferential peak strain; (G/S/L)CTTPS, (global/septal/lateral) circumferential time to peak strain; (G/S/L)LPS, (global/septal/lateral) longitudinal peak strain; (G/S/L)LTTPS, (global/septal/lateral) longitudinal time to peak strain; ICC, intraclass correlation coefficient; LV-2CH, left ventricular two-chamber view; LV-4CH, left ventricular four-chamber view; LV-SAX, left ventricular short-axis view; MRI, magnetic resonance imaging; ST, speckle tracking; TAG, tagging; US, ultrasound.

Yentl Brandt and Jolijn M. Lubrecht shared first authorship.

This is an open access article under the terms of the [Creative Commons Attribution-NonCommercial-NoDerivs](https://creativecommons.org/licenses/by-nc-nd/4.0/) License, which permits use and distribution in any medium, provided the original work is properly cited, the use is non-commercial and no modifications or adaptations are made.

© 2024 The Authors. *NMR in Biomedicine* published by John Wiley & Sons Ltd.

between imaging techniques. MRI feature tracking shows adequate comparability with ultrasound speckle tracking.

**KEYWORDS**

cardiac ultrasound, feature tracking, magnetic resonance imaging, myocardial strain, speckle tracking, tagging, validation

## 1 | INTRODUCTION

Quantification of myocardial strain enables the assessment of myocardial deformation throughout the cardiac cycle, providing insights into cardiac function.

The first method that was developed to measure systolic left ventricle myocardial strain was magnetic resonance imaging tagging (MRI-TAG).<sup>1,2</sup> MRI-TAG uses true tissue markers (tags), in the form of a grid-like pattern, to track myocardial deformation. Using a dedicated MRI-TAG sequence, additional radiofrequency pulses are applied to generate these tags. This MRI sequence is acquired in addition to the routinely acquired cardiac cine-MR images. A few disadvantages of MRI-TAG have hampered its broad application in clinical practice. With MRI-TAG, typically only 1–3 cross-sectional slices are acquired to quantify radial and circumferential strain. Increasing the number of slices or the acquisition of images in the long-axis plane to quantify longitudinal strain is technically feasible, but is impractical because of long scan times. Other downsides include tag deposition delay and tag fading. Tag deposition occurs with a delay of  $\approx 30$  ms after R wave detection.<sup>3</sup> Therefore, the physiological start of the systolic phase is slightly misidentified, which leads to a slight underestimation of peak strain. Tag fading refers to the decreased visibility of the tags over time, which hampers strain assessment in the diastolic phase.

Alternatively, two other methods to quantify myocardial strain have been developed that are more easily applicable in clinical practice, ultrasound speckle tracking (US-ST)<sup>4,5</sup> and MRI feature tracking (MRI-FT). These methods use conventional echocardiography images (US-ST) or conventional cine-MR images (MRI-FT) to calculate strain, eliminating the need to acquire an additional MRI sequence.<sup>6</sup>

With US-ST, naturally occurring speckled patterns of the signal intensity on the ultrasound images are tracked to calculate strain. Cardiac ultrasonography is readily available and applicable in standard clinical care and does not suffer from the comparatively long scan times required for MRI. US-ST supersedes MRI-TAG and MRI-FT in terms of temporal resolution<sup>7</sup> with the acquisition of  $\approx 50$  phases per cardiac cycle. However, the image quality is highly dependent on operator skill, and a plethora of other factors.

Similar to US-ST, MRI-FT is based on the tracking of specific naturally occurring signal intensity patterns (features) in cine-MR images. MRI-FT has a higher temporal resolution compared with MRI-TAG. For MRI-TAG, typically  $\approx 16$  cardiac phases are acquired, while for cine-MRI (MRI-FT) this number is typically  $\approx 30$ . Because MRI-FT and US-ST are not based on tags that fade over the cardiac cycle, the diastolic strain can be quantified as well.

Other MRI strain methods have also been developed, that is, fast strain-encoded MRI (fast-SENC)<sup>8</sup> and displacement encoding with stimulated echoes (DENSE).<sup>9</sup> Both techniques have a higher spatial resolution than MRI-TAG, and fast-SENC allows for acquisition in one heartbeat. Because these techniques require additional sequences, and suffer from a lower temporal resolution compared with MRI-FT, they are not applied in routine clinical practice.<sup>3</sup>

While MRI-TAG has been extensively validated,<sup>10,11</sup> this is less the case for MRI-FT and US-ST. Therefore, MRI-TAG is the gold standard method and MRI-FT and US-ST are still not routinely used in clinical practice. To validate these techniques, we aim to perform a direct comparison of cardiac circumferential strain and time-to-peak strain acquired via MRI-TAG and MRI-FT in two retrospective patient studies in formerly pre-eclamptic women, women with a history of normotensive pregnancy, and left bundle branch block (LBBB) patients. Next, we will perform an indirect comparison of the longitudinal strain measurements from MRI-FT and US-ST in the same patient studies.

## 2 | EXPERIMENTAL

### 2.1 | Study population

The study cohort comprised 22 patients with LBBB, and 20 participants from the DEcreased Cognitive functiON, NEurovascular CorrelaTions, and myocardial changes in women with a history of preeclampsia (DECONNECT) study (17 women with a history of preeclampsia and three healthy female controls), who were recruited from two prospective studies conducted at the Maastricht University Medical Centre (MUMC+): the 4D-flow in LBBB study (local ethical approval: NL59828.068.16) and the DECONNECT study (local ethical approval: NL47252.068.14). The DECONNECT study is registered at [clinicaltrials.gov](https://clinicaltrials.gov) with the identifier number NCT02347540. All LBBB patients underwent cardiac MRI and

cardiac ultrasound on the same day as part of the study protocols, whereas the formerly preeclamptic women and healthy female controls had varying time intervals between these two examinations (mean interval:  $15 \pm 9$ , range: 2–32 months). The participants in the DECONNECT study had a slightly higher heart rate during the cardiac MRI examination (mean difference  $6.4 \pm 11$  BPM,  $p = 0.02$ ). In the LBBB patient population, heart rates did not differ between ultrasound and cardiac MRI acquisitions (mean difference  $-2.5 \pm 8.6$  BPM,  $p = 0.26$ ). None of the patients had an adverse cardiac event in the period between the MRI and ultrasonography examination. All subjects provided oral and written informed consent before study participation in both studies.

## 2.2 | Data acquisition

### 2.2.1 | Cardiac MRI

For both studies, cardiac MRI data were acquired on the same 3-T MRI system (Ingenia, Philips Healthcare, Best, The Netherlands) using a phased-array torso radiofrequency coil (dStream, Philips Healthcare, Best, The Netherlands). A steady-state free precession sequence was used to obtain electrocardiogram (ECG)-gated cine images in the left ventricular (LV) two- and four-chamber long-axes and multislice short-axis views covering the entire left ventricle. The MRI acquisition parameters for the cine-MRI and the MRI-TAG sequences are provided in Table 1.

### 2.2.2 | Ultrasound

Standard echocardiograms were acquired using a Philips ultrasound system (all patients) (iE33, Philips Healthcare, Andover, MA, USA) using S-5 and X-5 transducers. Imaging parameters such as gain, depth setting, and contrast control varied according to the ultrasonographer's discretion.

## 2.3 | Study design

The cardiac MRI and cardiac ultrasound images of every patient were analyzed using the following three methods: MRI-TAG, MRI-FT, and US-ST. Circumferential strains were computed and compared using MRI-TAG and MRI-FT, whereas longitudinal strains were evaluated using MRI-FT and US-ST. Radial strains were not assessed because of low accuracy for radial strain in MRI-TAG analysis. Analysis was performed by two trained observers, who were responsible for all three analysis methods within either the LBBB or the DECONNECT patient groups. The observer of the DECONNECT group data was blinded for control/case status, and both observers were blinded for all clinical parameters. MRI-FT and MRI-TAG analyses were performed approximately 12 months after US-ST analysis for the DECONNECT group, removing the possibility of recollection of which group a subject belonged to. The first assessor (DECONNECT study) is formally trained in the acquisition and interpretation of clinical echocardiography (2 years of experience) and is trained by a clinical radiologist in MRI-FT contouring. The second observer (LBBB study) is specialized in cardiovascular biomechanics, with a formal training by clinical radiologists in medical imaging analysis, and is experienced in the use of MRI-TAG through special training by biomedical engineers and cardiologists.

With every method the peak strain and time to peak strain were determined using the imaging planes, as listed in Table 2. Peak strain was defined as the maximum shortening compared with end diastole, and the time to peak strain was defined as the point in time in which peak strain occurs. The end-diastolic phase was set as the reference value with a time of 0 ms. The peak strains and time to peak strains were compared within each patient to evaluate the correlation between the various methods.

## 2.4 | Data analysis

### 2.4.1 | MRI-TAG

Circumferential strain was determined from the cine-MRI and grid-tagged short axis images using custom software employing the SinMod method<sup>12</sup> implemented in the MATLAB environment (version R2022a; MathWorks, Natick, MA, USA).

The SinMod method tracks local displacement in a cross-sectional view of the left ventricle in a time series of MRI-TAG images. The method simultaneously detects local spatial phase shift and spatial frequency in bandpass-filtered images by modeling the environment of a pixel as a summation of sine wavefronts. From these waves, the component of displacement in every pixel is estimated by comparing the pixels in two images of consecutive cardiac phases, without the use of nearby pixels. Validation of this method has shown that the SinMod method performs equally

TABLE 1 Cardiac MRI acquisition parameters.

| Parameter                     | DECONNECT study      |                      |                      |            | LBBB study           |                      |                      |            |
|-------------------------------|----------------------|----------------------|----------------------|------------|----------------------|----------------------|----------------------|------------|
|                               | LV two-chamber       | LV four-chamber      | LV short axis        | Tagging    | LV two-chamber       | LV four-chamber      | LV short axis        | Tagging    |
| Pulse sequence                | SSFP                 | SSFP                 | SSFP                 | SSFP       | SSFP                 | SSFP                 | SSFP                 | SSFP       |
| Acquisition format            | 2D                   | 2D                   | 2D                   | 2D         | 2D                   | 2D                   | 2D                   | 2D         |
| TR (ms)                       | 2.7                  | 3.1                  | 3                    | 10         | 2.7                  | 3.1                  | 2.9                  | 5.3        |
| TE (ms)                       | 1.4                  | 1.5                  | 1.5                  | 5.5        | 1.4                  | 1.5                  | 1.4                  | 3.2        |
| Flip angle (°)                | 45                   | 45                   | 50                   | 10         | 45                   | 45                   | 50                   | 10         |
| No. of slices                 | 1                    | 1                    | 14                   | 3          | 1                    | 1                    | 12                   | 3          |
| No. of phases                 | 28                   | 28                   | 28                   | 16         | 30                   | 30                   | 30                   | 15–17      |
| Slice thickness (mm)          | 8                    | 8                    | 8                    | 8          | 8                    | 8                    | 8                    | 8          |
| Slice gap (mm)                | -                    | -                    | 2                    | 10         | -                    | -                    | 2                    | 10         |
| FOV (mm)                      | 350 × 350            | 350 × 350            | 350 × 350            | 300 × 300  | 350 × 350            | 350 × 350            | 350 × 350            | 300 × 300  |
| Acquisition matrix            | 176 × 216            | 176 × 210            | 160 × 215            | 152 × 124  | 176 × 201            | 176 × 197            | 160 × 264            | 200 × 170  |
| Acquired voxel size (mm)      | 2.0 × 1.6            | 2.0 × 1.7            | 2.2 × 1.3            | 2.0 × 2.2  | 2.0 × 1.6            | 2.0 × 1.6            | 2.2 × 1.3            | 1.5 × 1.8  |
| Reconstruction matrix         | 432 × 432            | 432 × 432            | 528 × 528            | 256 × 256  | 432 × 432            | 432 × 432            | 528 × 528            | 320 × 320  |
| Reconstructed voxel size (mm) | 0.8 × 0.8            | 0.8 × 0.8            | 0.7 × 0.7            | 1.2 × 1.2  | 0.8 × 0.8            | 0.8 × 0.8            | 0.7 × 0.7            | 0.9 × 0.9  |
| Parallel imaging factor       | 1.8                  | 1.8                  | 2                    | 1.5        | 1.8                  | 1.9                  | 1.7                  | 2          |
| ECG gating/triggering         | Retrospective gating | Retrospective gating | Retrospective gating | Triggering | Retrospective gating | Retrospective gating | Retrospective gating | Triggering |

Abbreviations: DECONNECT, DEcreased Cognitive functiON; NEurovascular CorrelaTees, and myocardial changes in women with a history of preeclampsia; ECG, electrocardiogram; FOV, field of view; LBBB, left bundle branch block; LV, left ventricular; MRI, magnetic resonance imaging; SSFP, steady-state free precession; TE, echo time; TR, repetition time.

**TABLE 2** Specification of the imaging planes for the three methods.

| Strain parameters | MRI-TAG                        | MRI-FT                     | US-ST                |
|-------------------|--------------------------------|----------------------------|----------------------|
| GC(TT)PS          | LV-SAX cine-MRI and tagged MRI | LV-SAX cine-MRI            |                      |
| S/LC(TT)PS        | LV-SAX cine-MRI and tagged MRI | LV-SAX cine-MRI            |                      |
| GL(TT)PS          |                                | LV-2CH and LV-4CH cine-MRI | LV-2CH and LV-4CH US |
| S/L(TT)PS         |                                | LV-4CH cine-MRI            | LV-4CH US            |

Abbreviations: GC(TT)PS, global circumferential (time to) peak strain; GL(TT)PS, global longitudinal (time to) peak strain; LV-2CH, left ventricular two-chamber view; LV-4CH, left ventricular four-chamber view; LV-SAX, left ventricular short-axis view; MRI, magnetic resonance imaging; MRI-FT, MRI feature tracking; MRI-TAG, MRI tagging; S/LC(TT)PS, septal/lateral circumferential (time to) peak strain; S/LL(TT)PS, septal/lateral longitudinal (time to) peak strain; US, ultrasound; US-ST, ultrasound speckle tracking.

well or better than the previously established harmonic phase method. In a standard gridline texture with a wavelength of six pixels, the residual mean square error is better than 0.02.<sup>12</sup>

The software automatically spatially matched the grid-tagged images to the cine-MR images in the x, y, and z directions to facilitate user-guided segmentation. Images that could not be matched in the longitudinal direction, due to a difference in slice position and/or orientation during acquisition, were excluded. In-plane patient movement between the acquisition of the cine- and tagged-MRI was corrected automatically.

Both the left and right ventricle were contoured, although for the purposes of this study, only LV information was used because of the inability of the MRI-FT and US-ST software packages used in the current study to assess right ventricular strain. The displacement field was divided into six segments according to the outer ring of the AHA bullseye and converted into Lagrangian strain (first frame, end-diastolic phase, as reference).

## 2.4.2 | MRI-FT

Longitudinal and circumferential strain measurements were obtained from the cine-MRI left ventricular four-chamber (LV-4CH), two-chamber (LV-2CH), and short-axis view images (LV-SAX) using the CAAS MR Solutions 5.2.1 software package (Pie Medical Imaging BV, Maastricht, The Netherlands). This software package utilizes feature tracking to extract longitudinal, circumferential, and radial strain from short and long axis cine-MRI.

After selection of the LV-4CH, LV-2CH, and LV-SAX images, a machine learning algorithm performed automatic segmentation of the LV endocardial and epicardial border and identified the end-diastolic and end-systolic phase, and the short axis basal and apical plane. The machine-learning algorithm is based on an established convolution neural network architecture, U-Net,<sup>13</sup> and uses four downward convolution layers. Separately trained networks exist for LV segmentation of LV-4CH, LV-2CH, and LV-SAX. The training was performed using LV annotations at end-diastole and end-systole on a multivendor, multicenter, and heterogeneous cohort of 520 patients. The inclusion of end-systolic annotations aims to increase input diversity.

Operator verification was performed to check the performance of the automatic LV segmentation, and the apical and basal plane identification, and manual adjustments were performed, when necessary. After operator approval, the deformation of the LV myocardium was tracked along the cardiac cycle based on registration of consecutive phases using a block-matching algorithm,<sup>14</sup> leading to a displacement vector for every pixel within the myocardium (Figure 1). Using the displacement vectors between each consecutive phase, the cumulative displacement of each pixel within the myocardium along the cardiac cycle was calculated. For illustration, the tracked path of the endocardial and epicardial boundaries is displayed. Based on the cumulative myocardium tissue displacement, the myocardial strain along the cardiac cycle was calculated relative to the end-diastolic phase. Three strain curves were calculated with respect to the primary axes of the left ventricle: the longitudinal, circumferential, and radial direction.

Furthermore, the displacement was also inspected by the observer to ensure correct tracking of the myocardial features over the course of the cardiac cycle. In case of improper tracking of the myocardial wall, a correction of the initial regions of interest was performed.

For a direct comparison, the circumferential peak strain and time to peak strain values of MRI-FT were extracted from the raw output files and matched slice-by-slice with the cine-MRI slices used by the SinMod software package.

## 2.4.3 | Cardiac US-ST

Longitudinal strain measurements were obtained from apical LV-2CH and LV-4CH ultrasound images using the Caas Qardia 1.0 software package (Pie Medical Imaging BV) that utilizes speckle tracking to extract longitudinal strain.

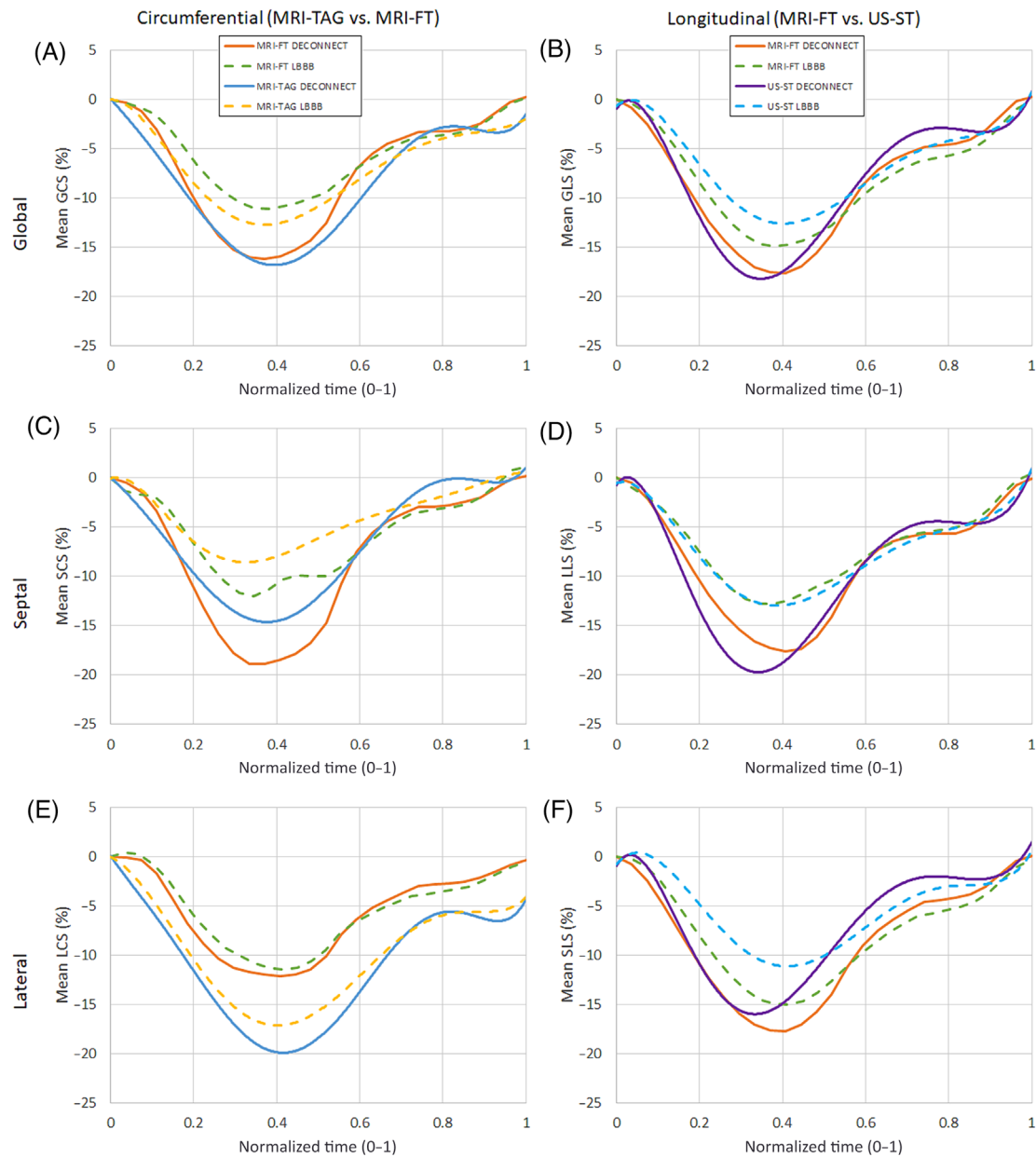


**FIGURE 1** Average peak strain values over normalized time (0–1) for the left bundle branch block (LBBB) patients and the subjects from the DECREASED COGNITIVE FUNCTION, NEUROVASCULAR CORRELATES, and MYOCARDIAL CHANGES IN WOMEN WITH A HISTORY OF PREECLAMPSIA (DECONNECT) study. MRI feature tracking (MRI-FT) values are averaged. MRI tagging (MRI-TAG) and ultrasound speckle tracking (US-ST) values are approximated with a sixth-degree polynomial regression line derived from all individual strain graphs. (A) Global circumferential strain (GCS), (B) Global longitudinal strain (GLS), (C) Septal circumferential strain (SCS), (D) Lateral longitudinal strain (LLS), (E) Lateral circumferential strain (LCS), (F) Septal longitudinal strain (SLS). MRI, magnetic resonance imaging.

The observer selected the appropriate images, whereafter three points were indicated on the end-diastolic image, that is, the left and right mitral annular hinge points and the LV apex, to guide the automated segmentation of the LV endocardial border. The end-diastolic image was automatically identified using ECG information through the DICOM metadata. The guided segmentation is based on a minimum cost algorithm.

Operator verification was performed to check the performance of the automatic LV segmentation and the contour was adjusted when necessary. After operator approval, the LV was tracked through the cardiac cycle using a speckle tracking algorithm based on normalized cross-correlation,<sup>15</sup> leading to an automatic calculation of the longitudinal displacement and strain (Figure 1).

## 2.5 | Statistical analysis

All strain values were compared at an inpatient level and are reported as maximal percentage shortening (peak strain) or milliseconds (time to peak strain) from the end-diastolic phase. The correlations between the various techniques were assessed using the intraclass correlation coefficient (ICC). ICC values less than 0.50 were considered as a poor correlation, 0.50–0.75 as moderate, 0.75–0.90 as good, and greater than 0.90 as excellent.<sup>16</sup> Correlations with a *p* value of less than 0.05 were considered significant. The inpatient agreement for two techniques was evaluated using Bland–Altman analysis, showing mean difference (bias) and the 95% limits of agreement. The significance of the bias between two techniques was evaluated using a two-sided paired samples *t*-test. *p* less than 0.05 was considered statistically significant. Normal distribution of the bias was assessed with a Kolmogorov–Smirnov test for normality and found to be normally distributed.

## 3 | RESULTS

For all 42 subjects, cine-MRI and tagging grid images were available. For six LBBB patients, ultrasound images were not acquired. During image analysis, 11 patients were excluded from MRI-TAG analysis because of incorrect slice positioning and/or orientation during the MRI acquisition. The MRI-TAG software package that was used in the current study prevents image analysis in the case of misregistration errors. Another patient was excluded from MRI-TAG analysis because of incomplete acquisition of the MRI-TAG images.

In total, data from 36 (16 LBBB, 20 DECONNECT) subjects were available for the longitudinal parameters, and data from 30 (16 LBBB, 14 DECONNECT) subjects were available for the circumferential parameters.

Figure 1 shows the average normalized strain–time curves for all three techniques for the two study populations. Good agreement can be observed for the global strain curves between the various techniques. In the segmental strain curves, differences between the techniques can be observed for the peak strain (for the circumferential and longitudinal direction) and the time to peak strain values (for the longitudinal direction, DECONNECT group), with the exception of septal longitudinal peak strain (SLPS) measured in the LBBB group, which showed excellent agreement. On average, LBBB patients have a lower absolute value of myocardial strain on both a global and segmental level.

Figure 2 provides typical examples of individual strain–time curves for global circumferential strain and global longitudinal strain (GLS) for all techniques for the DECONNECT and LBBB groups. It can be observed that the strain–time curves for the various techniques are very similar, although the absolute value of the GLS is slightly higher for MRI-FT versus US-ST for the LBBB group.

Figure 3 provides an example of typical images of the end-diastolic and end-systolic phases acquired with the three techniques, with and without the segmentation and displacement paths. Image quality varied between acquisitions, with MRI-TAG showing tag fading towards the end of the cardiac cycle. Furthermore, the MRI-TAG software package used in this study does not show contours or tracking over the entire cardiac cycle. The cine-MR images that were used for MRI-FT had good image quality. It can be observed that the features could be tracked over the entire cardiac cycle. US-ST image quality varied between individuals, but contour assessment deemed the speckle tracking to be sufficient for image analysis.

Figures 4–7 represent the ICC and Bland–Altman plots of the circumferential and longitudinal peak strain and time to peak strain.

Global circumferential peak strain (GCPS), compared between MRI-FT and MRI-TAG (Figure 4), showed good correlation (ICC = 0.83, 95% CI = 0.63–0.92, *p* < 0.01) with no significant bias. Septal circumferential peak strain (SCPS) showed moderate correlation (ICC = 0.74, 95% CI = 0.45–0.88, *p* < 0.01) with a significant overestimation by MRI-FT ( $-4.0\% \pm 4.7\%$ , *p* < 0.01). Lateral circumferential peak strain (LCPS) showed moderate correlation (ICC = 0.62, 95% CI = 0.20–0.82, *p* < 0.01) with a significant underestimation ( $7.4\% \pm 3.4\%$ , *p* < 0.01) by MRI-FT.

Global circumferential time to peak strain (GCTPS), compared between MRI-FT and MRI-TAG (Figure 5), showed good correlation (ICC = 0.82, 95% CI = 0.63–0.92, *p* < 0.01) with no significant bias. Septal and lateral circumferential time to peak strain showed moderate correlation (ICC = 0.74, 95% CI = 0.46–0.88, *p* < 0.01, and ICC = 0.74, 95% CI = 0.45–0.87, *p* < 0.01 for septal and lateral values, respectively) with no significant bias.

Global longitudinal peak strain (GLPS), compared between MRI-FT and US-ST (Figure 6), showed moderate correlation (ICC = 0.71, 95% CI = 0.43–0.85, *p* < 0.01) with no significant bias. SLPS showed good correlation (ICC = 0.77, 95% CI = 0.55–0.88, *p* < 0.01) with a significant overestimation by US-ST ( $1.8\% \pm 3.5\%$ , *p* < 0.01). Lateral longitudinal peak strain (LLPS) showed poor correlation (ICC = 0.23, 95% CI =  $-0.51$ –0.61, *p* = 0.22) with a significant underestimation by US-ST ( $-2.2\% \pm 4.3\%$ , *p* < 0.01).

Global longitudinal time to peak strain (GLTTPS), compared between MRI-FT and US-ST (Figure 7), showed moderate correlation (ICC = 0.56, 95% CI = 0.14–0.78, *p* < 0.01) with no significant bias. Septal (SLTTPS) and lateral longitudinal time to peak strain (LLTTPS) showed moderate correlations (ICC = 0.58, 95% CI = 0.18–0.79, *p* < 0.01, and ICC = 0.70, 95% CI = 0.42–0.85, *p* < 0.01 for septal and lateral values, respectively) with no significant biases.

Table 3 gives an overview of the average strain values per imaging method and per study population, at global, septal, and lateral levels. Comparison within the DECONNECT group showed that, for all three techniques, the healthy controls (*n* = 3) had, on average, higher absolute strain values than the formerly preeclamptic women (*n* = 17), although in these small groups this result was not statistically significant. All three

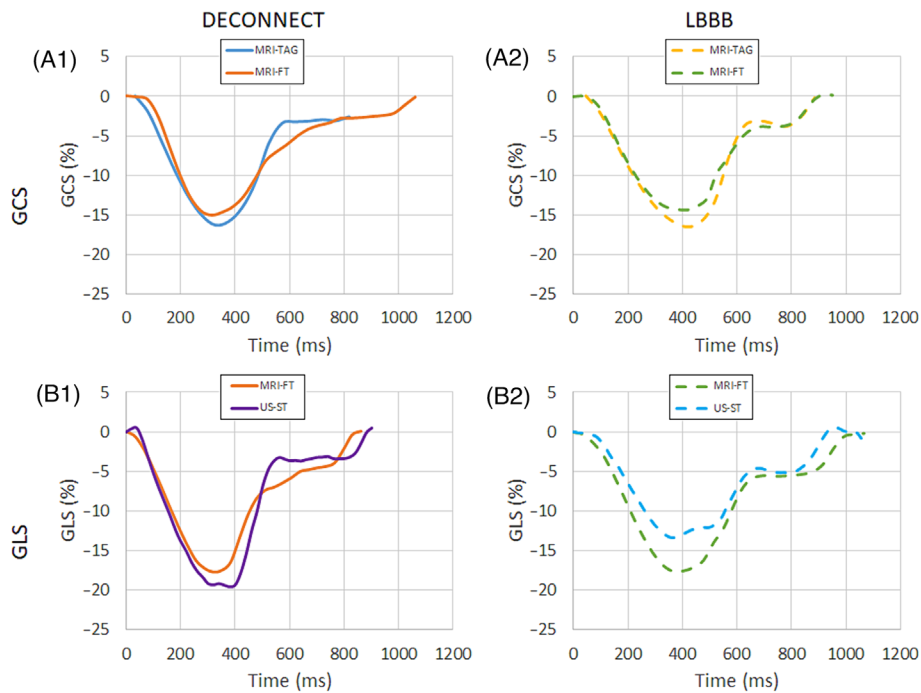


**FIGURE 2** Typical strain–time curves for global circumferential strain (A1 and A2) and global longitudinal strain (B1 and B2) for all techniques, for one subject each from the DECONNECT and the LBBB group. GCS, global circumferential strain; GLS, global longitudinal strain; MRI, magnetic resonance imaging; MRI-FT, MRI feature tracking; MRI-TAG, MRI tagging; US-ST, ultrasound speckle tracking.

techniques were able to measure differences in strain values between the DECONNECT and the LBBB group, apart from LCPS (MRI-TAG and MRI-FT), SLTTPS (MRI-FT and US-ST), and GLTTPS (US-ST).

For the subjects in the DECONNECT study, the heart rate during the cardiac MRI examination was slightly higher than that for the echocardiography examination ( $6 \pm 11$  BPM,  $p = 0.02$ ). Assessment through univariable linear regression indicated no association between heart rate and GLPS ( $\beta = 0.002\%$ ,  $p = 0.94$ ), SLPS ( $\beta = 0.007\%$ ,  $p = 0.87$ ), and LLPS ( $\beta = -0.049\%$ ,  $p = 0.22$ ) in the DECONNECT study population. There was an association with heart rate and GLTTPS ( $\beta = -2$  ms,  $p < 0.01$ ), SLTTPS ( $\beta = -2$  ms,  $p = 0.01$ ), and LLTTPS ( $\beta = -3$  ms,  $p < 0.01$ ). Given the average difference in BPM between examinations of 6 ms, this would lead to an approximate difference in LLTTPS of  $-18$  ms, which is slightly below the temporal resolution of US-ST ( $\sim 20$  ms).

## 4 | DISCUSSION

We have demonstrated predominantly moderate to good correlations between global as well as segmental LV peak strain and time to peak strain values obtained with MRI-FT versus MRI-TAG and US-ST versus MRI-FT. While no biases in absolute global strain values were observed, the segmental peak strains demonstrated a bias between MRI-TAG and MRI-FT, and US-ST and MRI-FT. This bias needs to be taken into account when comparing absolute values acquired with different imaging or acquisition techniques. The longitudinal peak strain in the lateral wall measured by US-ST did not show a significant correlation when compared with MRI-FT. No bias was observed for all time to peak strain values at global as well as segmental levels.

The agreement between MRI-TAG and MRI-FT for the global strain parameters that was observed in this study for GCPS and GCTTPS (0.83 [0.63–0.92] and 0.82 [0.63–0.92], respectively) is better than those in other studies.<sup>17–19</sup> Wu et al. reported ICC values of 0.58 (moderate) ( $p < 0.01$ ) and 0.38 (poor) ( $p = 0.02$ ) for GCPS and GCTTPS, respectively, with respective biases of  $3.5\% \pm 1.7\%$  ( $p < 0.01$ ) and  $24 \pm 22$  ms ( $p = 0.02$ )<sup>17</sup> in a study population consisting of healthy volunteers, LBBB and hypertrophic cardiomyopathy patients ( $n = 10$  for all). Bucius et al. reported an  $r$  value of 0.85,  $p$  less than 0.01, and a bias of 6.92% for GCPS<sup>18</sup> in a smaller population of healthy controls ( $n = 11$ ) and heart failure patients ( $n = 7$ ). Backhaus et al. found an agreement between MRI-FT and MRI-TAG for GCPS ranging from poor to good (ICC 0.41–0.85) and a significant bias between 0.8% and 9.4%, depending on the software package,<sup>19</sup> in a study population of healthy controls and heart failure patients ( $n = 12$  for both).



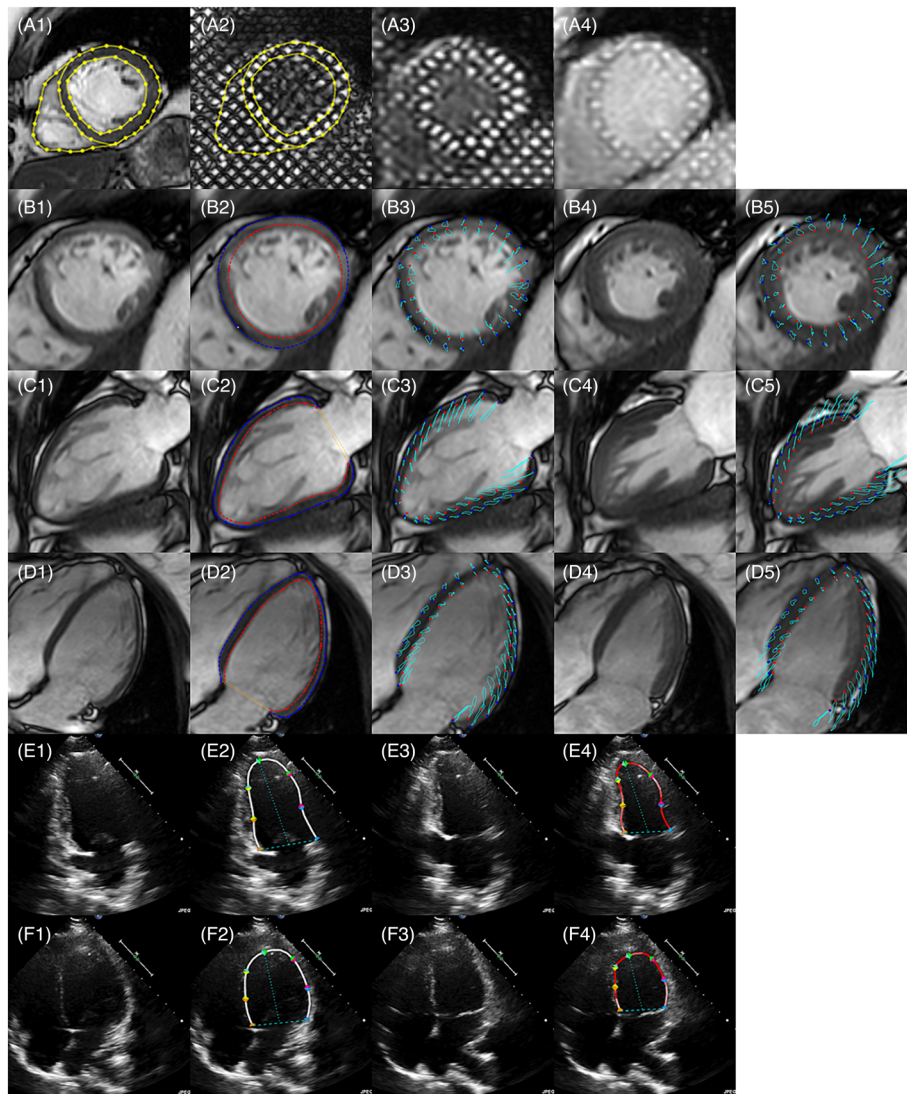


**FIGURE 3** Multiphase images for MRI tagging (MRI-TAG) (row A, including a coregistered cine-MRI with endocardial and epicardial contours [A1], the superimposed endocardial and epicardial contours on the tagging image [A2], an end-systolic image [A3], and a late-diastolic image [A4]), MRI feature tracking (MRI-FT) (rows B [short-axis], C [two-chamber], and D [four-chamber], including an end-diastolic cine-MR image [Column 1], end-diastolic endocardial and epicardial contours [Column 2], the displacement paths projected on the end-diastolic image [Column 3], end-systolic cine-MR image [Column 4], and the displacement paths projects on the end-systolic image [Column 5]), and US-ST (rows E [two-chamber] and F [four-chamber], including an end-diastolic image [Column 1], end-diastolic endocardial contours [Column 2], end-systolic image [Column 3], and end-systolic endocardial contours [Column 4]). Red contours in rows E and F, Column 4 indicate longitudinal shortening in that segment. MRI, magnetic resonance imaging; US-ST, ultrasound speckle tracking.

A multicenter study by Amzulescu et al. directly compared MRI-TAG with US-ST. In a study population of 136 patients, global and regional subendocardial longitudinal strain was assessed. GLS correlated highly between methods ( $ICC = 0.81$ ,  $p < 0.001$ ), but showed a significant bias ( $-37\% \pm 27\%$ ,  $p < 0.001$ ). Regionally, ICC values ranged from 0.17 to 0.81, with biases ranging from  $-9\%$  to  $-98\%$ .<sup>20</sup> This lower performance in regional compared with global strain has been described as an inherent drawback of strain assessment.<sup>20,21</sup> Small errors may occur, for example, because of out-of-plane effects. These errors are typically random and, therefore, average out when calculating the global strain. Regional values, however, are based on the average value over a smaller number of segments, leading to a more pronounced effect of these subtle errors.<sup>22</sup>

When comparing our findings with previous reports on segmental circumferential strain values, our study showed stronger correlations. We found moderate-to-good correlations ( $ICCs \geq 0.62$ ), while Wu et al. reported poor to moderate correlations (circumferential peak strain:  $ICC: 0.06-0.57$ , circumferential time to peak strain:  $ICC: -0.13-0.72$ ).<sup>17</sup> Moreover, van Everdingen et al. demonstrated moderate correlations for segmental peak strains ( $ICCs: 0.54-0.58$ ) and poor correlations for segmental time to peak strain ( $ICC: 0.17-0.34$ ),<sup>23</sup> which may be explained by their study population of 27 cardiac resynchronization therapy candidates. However, the bias that we observed in segmental peak strains was relatively high (absolute mean differences between  $-4.0\% \pm 4.7\%$  and  $7.4\% \pm 3.4\%$  for SCPS and LCPS, respectively), which may be explained by

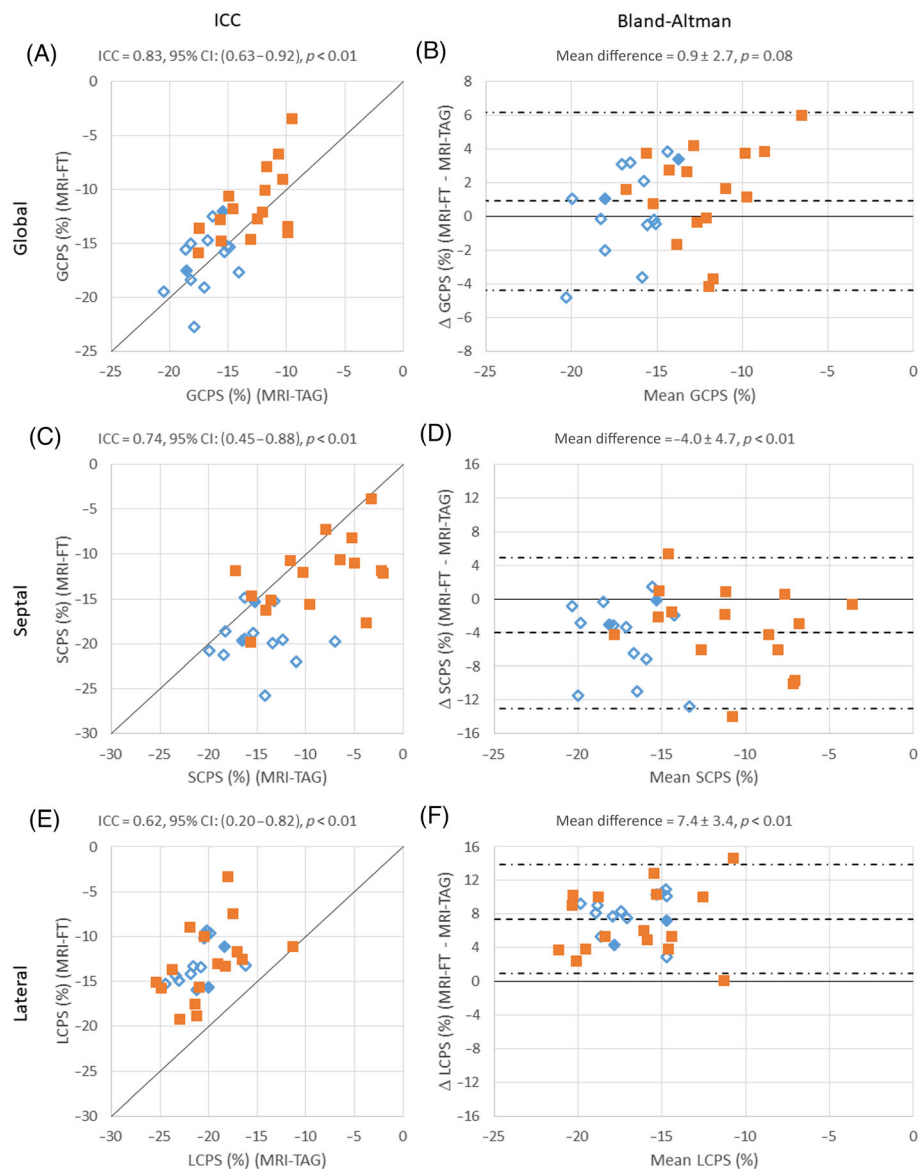


**FIGURE 4** Comparison of circumferential peak strain (CPS) parameters between MRI feature tracking (MRI-FT) and MRI tagging (MRI-TAG). CI, confidence interval; GCPS, global circumferential peak strain; ICC, intraclass correlation coefficient; LCPS, lateral circumferential peak strain; MRI, magnetic resonance imaging; SCPS, septal circumferential peak strain. Orange squares indicate left bundle branch block (LBBB) patients. Open blue diamonds indicate formerly preeclamptic DECONNECT patients and closed blue diamonds indicate controls with a history of normotensive pregnancy. The diagonal lines in (A), (C), and (E) represent the identity line. The dashed lines in (B), (D), and (F) represent the mean difference (bias). Dash-dotted lines in (B), (D), and (F) represent the 95% CI of the mean difference. Full lines in (B), (D), and (F) represent the  $y = 0$  lines.

differences in the study population. Therefore, we recommend using a single technique within the same study. In addition, the bias should be taken into consideration when comparing different studies.

Earlier studies comparing feature and speckle tracking describe moderate correlations for GLPS (Pearson correlation of 0.83,  $n = 106$  patients with varying cardiovascular diseases,<sup>24</sup> Pearson correlation of 0.74,  $n = 50$  patients with varying cardiovascular diseases,<sup>25</sup> and  $ICC = 0.67$ ,  $n = 100$  patients with former acute myocardial infarction<sup>26</sup>). In some studies, a significant bias is reported up to an absolute value of  $-3.1\%$ ,<sup>24,25</sup> while another study did not find a significant bias.<sup>26</sup> These findings are comparable with our results in terms of correlation ( $ICC = 0.71$  [0.43–0.85]), whereas no bias was detected in our global longitudinal parameters. Potential differences in results may be explained by differences in study populations.

In contrast to other parameters, LLPS, as quantified with MRI-FT and US-ST, showed no significant correlation and a significant bias. We observed that in several cases (in both populations) the ultrasound image quality of the lateral wall was lower than that of the septal wall, which may hamper correct speckle tracking over the cardiac cycle.

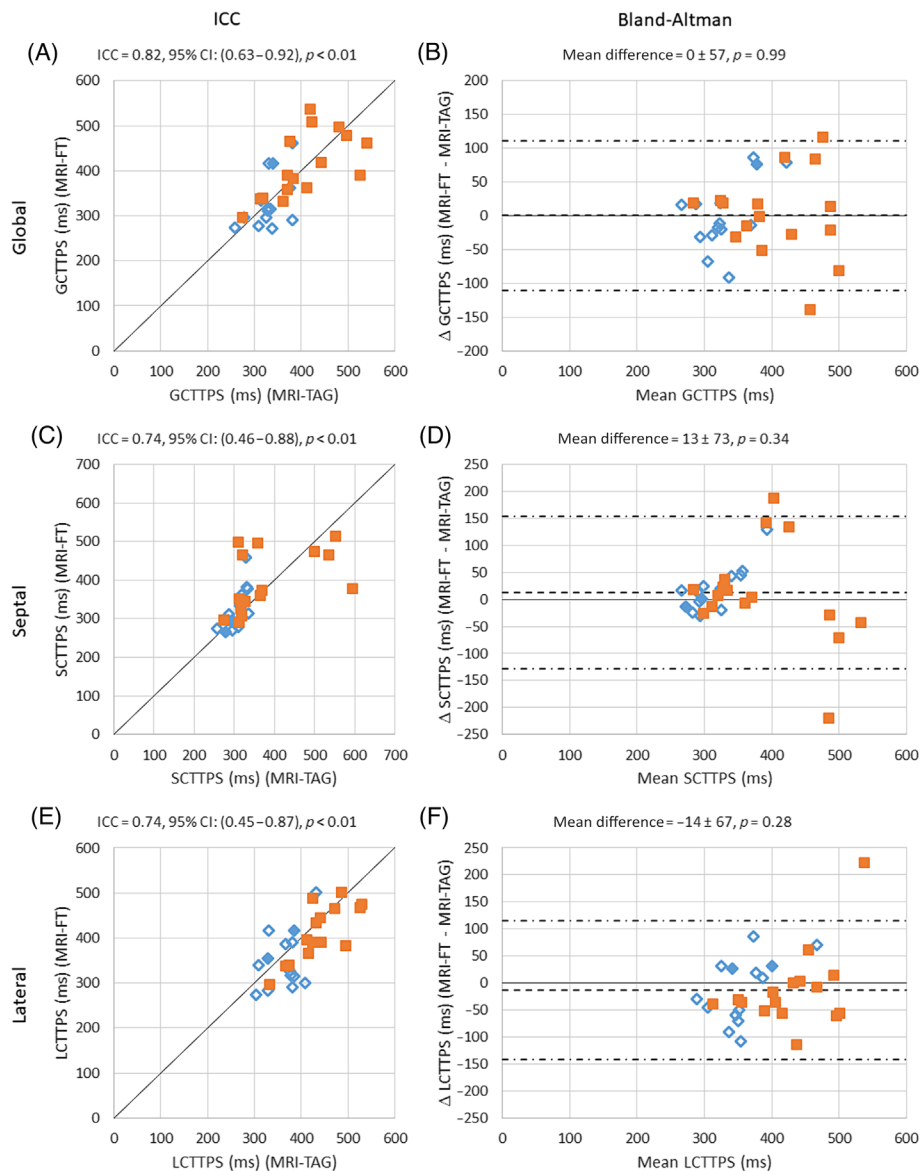


**FIGURE 5** Comparison of circumferential time to peak strain (CTTPS) parameters between MRI feature tracking (MRI-FT) and MRI tagging (MRI-TAG). CI, confidence interval; GCTTPS, global circumferential time to peak strain; ICC, intraclass correlation coefficient; LCTTPS, lateral circumferential time to peak strain; MRI, magnetic resonance imaging; SCTTPS, septal circumferential time to peak strain. Orange squares indicate left bundle branch block (LBBB) patients. Open blue diamonds indicate DECREASED Cognitive function, NEurovascular Correlates, and myocardial changes in women with a history of preeclampsia (DECONNECT) formerly preeclamptic patients and closed blue diamonds indicate controls with a history of normotensive pregnancy. The diagonal lines in (A), (C), and (E) represent the identity line. The dashed lines in (B), (D), and (F) represent the mean difference (bias). Dash-dotted lines in (B), (D), and (F) represent the 95% confidence interval of the mean difference. Full lines in (B), (D), and (F) represent the  $y = 0$  lines.

In summary, our results were comparable or better than previously reported findings in prior validation studies. Differences may be due to differences in patient populations between the studies or the use of other software packages. Our results expand the existing body of literature to women with a history of preeclampsia, as well as LBBB patients. Furthermore, we have shown that the image quality and analysis software performance for all techniques is sufficient for the assessment of circumferential and/or longitudinal strain on a global level. Segmental strain, however, remains biased between methods. Our comparatively better results on a global level may also be due to the fact that our analyses were performed by one observer per patient group, removing any interobserver effects on image segmentation. In previous strain validation studies, the primary image analysis was performed by either a single observer<sup>19,24</sup> or multiple observers.<sup>21,25</sup> In five studies, the number of observers was not provided.<sup>17,18,20,23,26</sup>

Another source of bias in our study could be related to differences in peak strain in the subendocardial and subepicardial layer that have been previously described.<sup>27,28</sup> MRI-TAG calculates strain based on the deformation of tags, which are typically equally distributed over the different

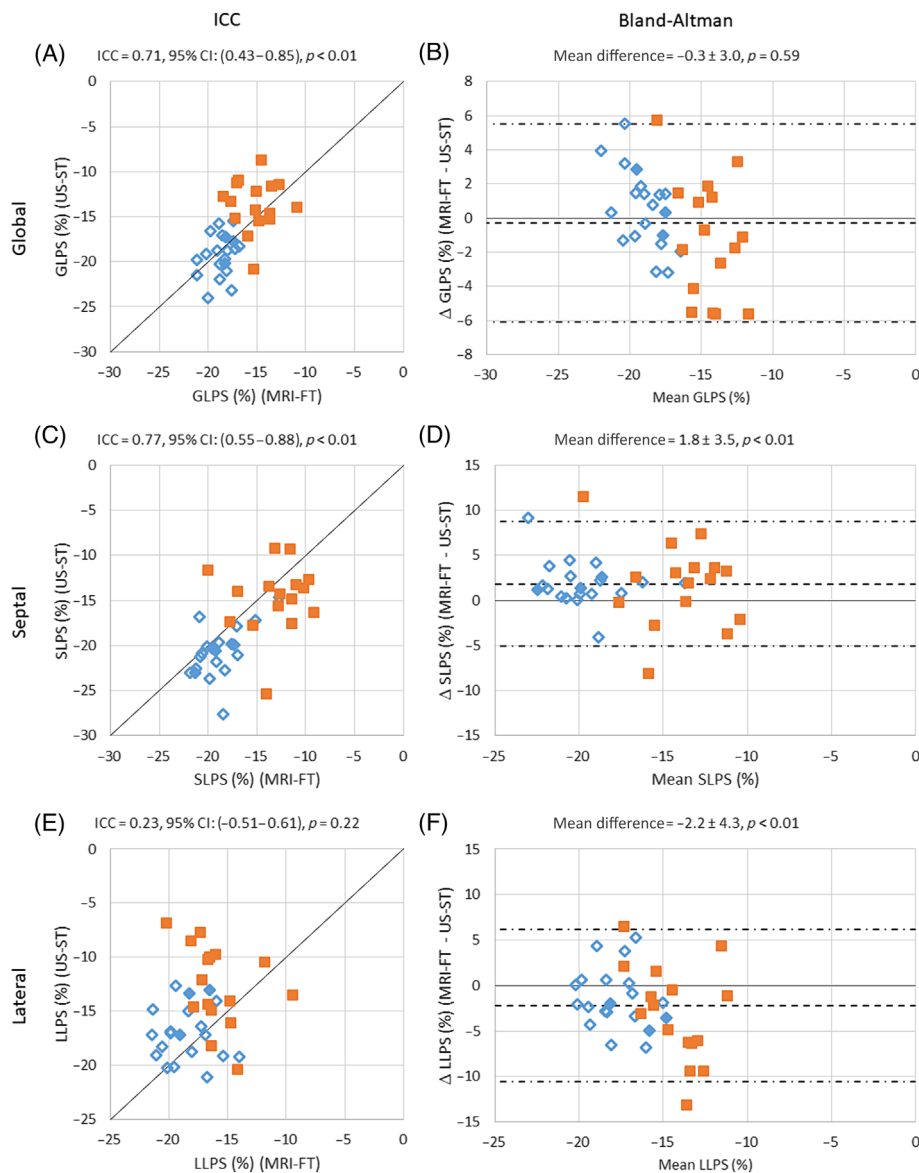


**FIGURE 6** Comparison of longitudinal peak strain (LPS) parameters between MRI feature tracking (MRI-FT) and ultrasound speckle tracking (US-ST). CI, confidence interval; GLPS, global longitudinal peak strain; ICC, intraclass correlation coefficient; LLPS, lateral longitudinal peak strain; MRI, magnetic resonance imaging; SLPS, septal longitudinal peak strain. Orange squares indicate left bundle branch block (LBBB) patients. Open blue diamonds indicate DECREASED Cognitive function, NEurovascular Correlates, and myocardial changes in women with a history of preeclampsia (DECONNECT) formerly preeclamptic patients and closed blue diamonds indicate controls with a history of normotensive pregnancy. The diagonal lines in (A), (C), and (E) represent the identity line. The dashed lines in (B), (D), and (F) represent the mean difference (bias). Dash-dotted lines in (B), (D), and (F) represent the 95% confidence interval of the mean difference. Full lines in (B), (D), and (F) represent the  $y = 0$  lines.

layers of the myocardial wall. The US-ST software package that we used in the current study creates an extrapolated continuous estimate of the endocardial border, resulting in an endocardial strain measurement. MRI-FT, as assessed with the software package that was used in the current study, makes use of both endocardial and epicardial contours, after which the strain results are averaged, giving a mean value of the entire myocardial wall.

Image quality varied between modalities and techniques (Figure 3). Tagging acquisitions showed excellent quality in the initial phases of the cardiac cycle, but tag fading was visible towards the diastolic phase, in line with previous studies.<sup>29</sup> Cine-MRI acquisitions were of excellent quality and remained interpretable throughout the entire cardiac cycle. Ultrasound acquisitions varied in quality, depending on the patient's physical disposition, the operator's experience, and the acquisition parameters. The excellent quality of cine-MR images makes MRI-FT suitable for strain assessment over the entire cardiac cycle.<sup>30</sup> The variation in echocardiographic image quality is a limitation of this technique.

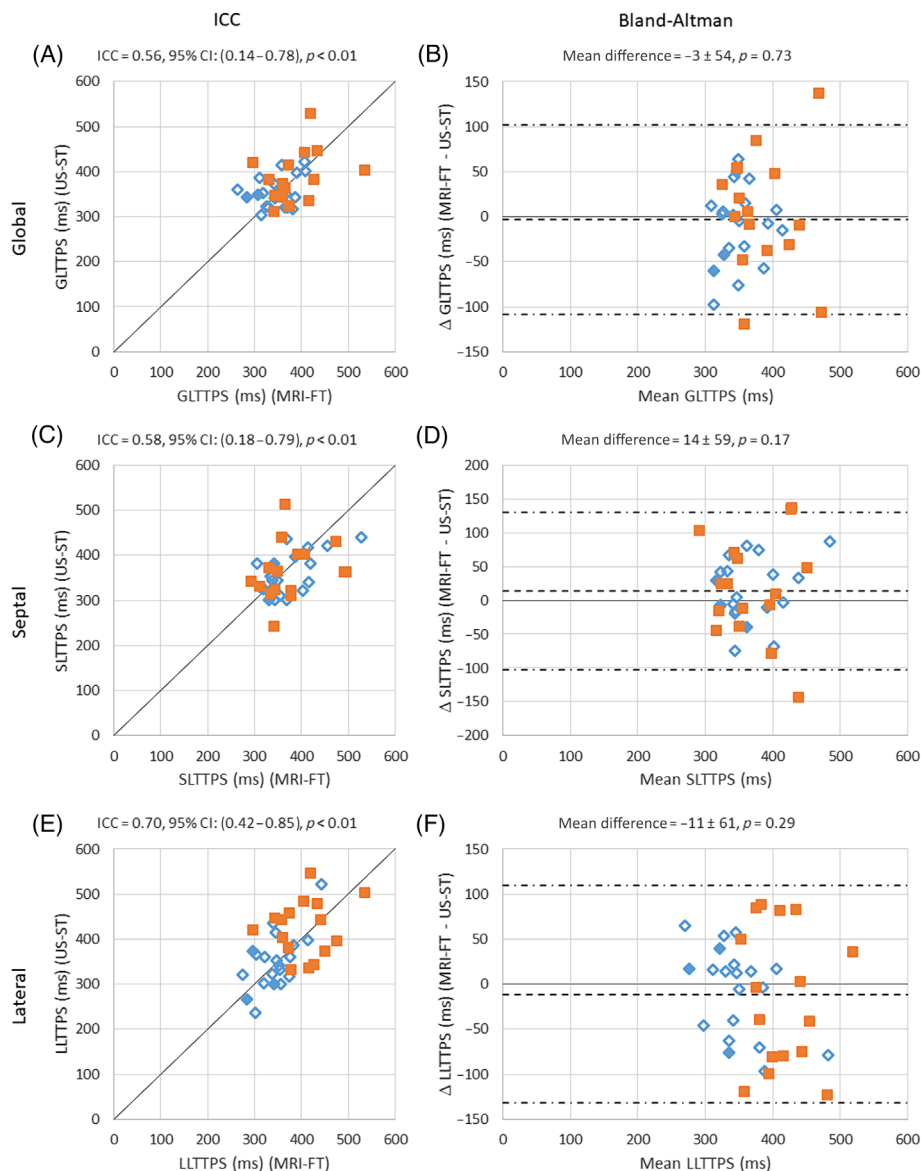


**FIGURE 7** Comparison of longitudinal time to peak strain (LTPS) parameters between MRI feature tracking (MRI-FT) and ultrasound speckle tracking (US-ST). CI, confidence interval; GLTTPS, global longitudinal time to peak strain; ICC, intraclass correlation coefficient; LLTTPS, lateral longitudinal time to peak strain; MRI, magnetic resonance imaging; SLTTPS, septal longitudinal time to peak strain. Orange squares indicate left bundle branch block (LBBB) patients. Open blue diamonds indicate formerly preeclamptic DECREASED COGNITIVE FUNCTION, NEUROVASCULAR CORRELATES, and MYOCARDIAL CHANGES IN WOMEN WITH A HISTORY OF PREECLAMPSIA (DECONNECT) patients and closed blue diamonds indicate controls with a history of normotensive pregnancy. The diagonal lines in (A), (C), and (E) represent the identity line. The dashed lines in (B), (D), and (F) represent the mean difference (bias). Dash-dotted lines in (B), (D), and (F) represent the 95% confidence interval of the mean difference. Full lines in (B), (D), and (F) represent the  $y = 0$  lines.

In the current study, we did not validate other MRI-based techniques to quantify myocardial strain, that is, SENC and DENSE. However, this was performed in previous studies. A comparison between MRI-TAG and SENC in a small cohort of 11 healthy controls and seven heart failure patients showed a good-to-excellent correlation between MRI-TAG, MRI-FT, and SENC (MRI-TAG vs. SENC:  $r = 0.858$ ,  $p < 0.001$ ; MRI-TAG vs. MRI-FT:  $r = 0.894$ ,  $p < 0.001$ ; MRI-FT vs. SENC:  $r = 0.924$ ,  $p < 0.001$ ).<sup>18</sup> This study also demonstrated that SENC overestimated longitudinal peak strain (LPS) and circumferential peak strain (CPS) compared with MRI-TAG (19.4% [17.1%–20.7%] vs. 14.9% [11.8%–16.9%] and 20.3% [16.5%–22.3%] vs. 17.8% [16.4%–19.5%] for LPS and CPS, respectively;  $p < 0.05$  for both). In addition, this study reported that MRI-FT overestimated the strain values to an even larger extent (23.5% [22.0%–25.9%] and 26.1% [21.8%–27.8%] for CPS and LPS, respectively;  $p < 0.05$  for both).

DENSE was validated by a direct comparison with MRI-TAG in a cohort of 10 healthy controls and 77 cardiac patients.<sup>30</sup> A good correlation was reported for CPS (ICC = 0.778), while the correlations for radial peak strain and LPS were poor (ICC = 0.032 and 0.359 for radial peak strain

TABLE 3 Overview of mean strain parameter values per modality and group.

|       | Differences in strain values between techniques in the DECONNECT population |   |   |   | Differences in strain values between techniques in the LBBB population |   |   |                          |
|-------|---|---|---|---|--|---|---|--------------------------|
|       | MRI-TAG   | MRI-FT                                    | US-ST                                     | p   | MRI-TAG  | MRI-FT                                    | US-ST                                     | p                        |
|       | CPS   | Global<br>Septal<br>Lateral               | -16.9 ± 1.8<br>-14.9 ± 3.3<br>-20.8 ± 2.1 | -16.5 ± 2.9<br>-19.3 ± 2.9<br>-12.9 ± 2.4 | 0.55<br>< 0.01*<br>< 0.01*   | -12.9 ± 2.7<br>-8.9 ± 5.2<br>-20.0 ± 3.6  | -11.5 ± 3.3<br>-12.5 ± 4.1<br>-13.0 ± 4.2 | 0.08<br>0.01*<br>< 0.01* |
| CTTPS | Global<br>Septal<br>Lateral   | 330 ± 35<br>302 ± 23<br>364 ± 38          | 331 ± 60<br>322 ± 55<br>351 ± 64          | 0.95<br>0.13<br>0.44                      | 408 ± 76<br>382 ± 103<br>439 ± 55                                      | 408 ± 73<br>390 ± 79<br>425 ± 85          | 0.97<br>0.73<br>0.45                      |                          |
| LPS   | Global<br>Septal<br>Lateral   | -18.7 ± 1.2<br>-18.9 ± 2.3<br>-18.5 ± 2.1 | -19.2 ± 2.3<br>-20.7 ± 2.8<br>-17.0 ± 2.5 | 0.30<br>< 0.01*<br>0.06                   | -15.1 ± 2.0<br>-13.1 ± 3.1<br>-15.8 ± 2.6                              | -13.8 ± 2.9<br>-14.9 ± 3.8<br>-12.7 ± 3.8 | 0.16<br>0.16<br>0.03*                     |                          |
| LTPPS | Global<br>Septal<br>Lateral   | 346 ± 40<br>371 ± 55<br>343 ± 42          | 355 ± 34<br>359 ± 46<br>351 ± 63          | 0.36<br>0.24<br>0.50                      | 386 ± 55<br>379 ± 62<br>407 ± 57                                       | 382 ± 57<br>363 ± 63<br>422 ± 63          | 0.80<br>0.41<br>0.43                      |                          |

Abbreviations: CPS, circumferential peak strain; CTTPS, circumferential time to peak strain; DECONNECT, DECREASED Cognitive functiOn, NEurovascular CorrelaTes, and myocardial changes in women with a history of preeclampsia; LBBB, left bundle branch block; LPS, longitudinal peak strain; LTPPS, longitudinal time to peak strain; MRI, magnetic resonance imaging; MRI-FT, MRI feature tracking; MRI-TAG, MRI tagging; US-ST, ultrasound speckle tracking.

\*Statistically significant differences ( $p < 0.05$ ).

TABLE 3 (Continued)

|       | Differences in strain values between techniques in the combined population |   |   |                               | Differences in strain values between DECONNECT and LBBB populations |                               |                               |                               |
|-------|--|---|---|-------------------------------|---|-------------------------------|-------------------------------|-------------------------------|
|       | MRI-TAG  | MRI-FT                                    | US-ST                                     | p                             | MRI-TAG   | MRI-FT                        | US-ST                         | p (US-ST)                     |
|       | CPS  | -14.8 ± 3.1<br>-11.7 ± 5.3<br>-20.4 ± 3.0 | -13.9 ± 4.0<br>-15.7 ± 4.9<br>-13.0 ± 3.4 | 0.08<br>< 0.01*<br>< 0.01*    | < 0.01*<br>< 0.01*<br>0.98  | < 0.01*<br>< 0.01*<br>0.73    | < 0.01*<br>< 0.01*<br>0.01*   | < 0.01*<br>< 0.01*<br>< 0.01* |
| CTTPS | 372 ± 72<br>346 ± 85<br>404 ± 60   | 372 ± 77<br>359 ± 76<br>390 ± 84          | 0.99<br>0.34<br>0.28                      | < 0.01*<br>< 0.01*<br>< 0.01* | < 0.01*<br>< 0.01*<br>0.01*   | < 0.01*<br>< 0.01*<br>0.01*   | < 0.01*<br>< 0.01*<br>< 0.01* |                               |
| LPS   | -17.1 ± 2.4<br>-16.3 ± 3.9<br>-17.3 ± 2.7                                  | -16.8 ± 3.7<br>-18.1 ± 4.4<br>-15.1 ± 3.8 | 0.59<br>< 0.01*<br>< 0.01*                | < 0.01*<br>< 0.01*<br>< 0.01* | < 0.01*<br>< 0.01*<br>< 0.01*                                       | < 0.01*<br>< 0.01*<br>< 0.01* | < 0.01*<br>< 0.01*<br>< 0.01* |                               |
| LTPPS | 364 ± 51<br>375 ± 57<br>371 ± 58   | 367 ± 47<br>361 ± 54<br>383 ± 72          | 0.73<br>0.17<br>0.29                      | 0.02*<br>0.26<br>< 0.01*      | 0.02*<br>0.26<br>< 0.01*  | 0.05<br>0.44<br>< 0.01*       | 0.05<br>0.44<br>< 0.01*       |                               |

Abbreviations: CPS, circumferential peak strain; CTTPS, circumferential time to peak strain; DECONNECT, DECREASED Cognitive functiOn, NEurovascular CorrelaTes, and myocardial changes in women with a history of preeclampsia; LBBB, left bundle branch block; LPS, longitudinal peak strain; LTPPS, longitudinal time to peak strain; MRI, magnetic resonance imaging; MRI-FT, MRI feature tracking; MRI-TAG, MRI tagging; US-ST, ultrasound speckle tracking.

\*Statistically significant differences ( $p < 0.05$ ).

and LPS, respectively). In the same study, a bias was observed for LPS (mean difference = 4.886% [−2.986%–12.76%],  $p < 0.001$ ), while there was no bias for CPS. In another study comprising 12 healthy volunteers, CPS showed good correlation between DENSE and MRI-TAG ( $r = 0.87$ ).<sup>31</sup> In line with our findings, in a cohort of 161 cardiac patients, 99 healthy adults, and 45 healthy children and adolescents, a higher agreement was between techniques on global versus segmental level.<sup>32</sup> CPS values measured by DENSE and MRI-FT were found to agree moderately at global levels but poorly at segmental levels (ICC = 0.72 and ICC = 0.48, respectively). In the same study, DENSE was also compared with StrainNet, a deep learning model that predicts intramyocardial displacement from contour motion, and showed good agreement at both global and segmental levels (ICC = 0.87 and ICC = 0.75, respectively). DENSE was proven to be reproducible at an intrauser, interuser-same-site, interuser-different-site, interuser-human-deep-learning, interscan, and intersession level in a cohort of both healthy subjects ( $n = 60$ ) and heart disease patients ( $n = 21$ ), with an ICC of 0.74 or higher for CPS and LPS at both global and segmental levels.<sup>33</sup> Furthermore, deep learning-based segmentation methods have been shown to be applicable for the postprocessing of DENSE images, showing high agreement with user-assisted (machine learning segmentation with manual adjustment) contouring in a cohort of 38 patients with cardiac disease and 70 healthy controls. GCPS had a correlation of  $r = 0.99$ , and pooled segmental CPS values had correlations of  $r = 0.94$ , 0.97, and 0.93 for the basal, midventricular, and apical slices, respectively.<sup>34</sup> Together, these findings show good-to-moderate correlation for GCPS between DENSE and MRI-TAG, and that DENSE has good-to-excellent reproducibility.

The current study had several limitations. Because of the retrospective nature of the study, data acquisition was not fully standardized, and subtle differences were present in MRI acquisition parameters. On the other hand, in clinical practice, such differences in MRI acquisition parameters are common. Moreover, because long-axis MRI-TAG data were not acquired, no truly conclusive comparison of US-ST with the established gold standard was possible. Furthermore, right ventricular strain was not assessed because of the inability of the MRI-FT and US-ST software packages that were used to contour the right ventricle and calculate the right ventricular peak strain. In addition, mismatching of the slice position between MRI-TAG and MRI-FT in the longitudinal direction led to the exclusion of 11 patients because our MRI-TAG software does not allow analysis in the case of a slight image misregistration. Also, in our study we did not investigate the interobserver and intraobserver agreement. A final limitation is that each type of strain analysis was performed using a single algorithm. Certainly, for US-ST it is known that important differences in peak strain values may be found when using different software packages of different vendors. A study comparing nine different software packages found an absolute difference of 3.7% ( $p < 0.01$ ) between vendors,<sup>35</sup> whereas we found a highest mean difference of 2.2% for LLPS.

## 5 | CONCLUSION

The comparison of strain quantification of MRI-FT versus MRI-TAG and US-ST versus MRI-FT shows generally comparable results. An exception to the moderate-to-good correlations was the poor correlation between MRI-FT and US-ST for LLPS. No significant bias was observed for global peak strain and all time-to-peak strain values. By contrast, a significant bias was observed for all segmental peak strain values.

### ACKNOWLEDGMENTS

This retrospective study received no additional funding.

### CONFLICT OF INTEREST STATEMENT

Jean-Paul Aben is an employee of Pie Medical Imaging (Maastricht, The Netherlands). Furthermore, the proprietary software of Pie Medical Imaging (Maastricht, The Netherlands) was provided in a research agreement at no charge. In order to prevent potential conflicts of interest, one of the co-authors (Jean-Paul Aben), who works for a commercial entity, has only been consulted for technical specifications of their respective software packages. Furthermore, this author was not involved in the acquisition or analysis of the results. All other authors declare no other financial interests.

### DATA AVAILABILITY STATEMENT

The data that support the findings of this study are available on request from the corresponding author. The data are not publicly available due to privacy or ethical restrictions.

### ORCID

M. Eline Kooi  <https://orcid.org/0000-0001-7562-5724>

### REFERENCES

1. Zerhouni EA, Parish DM, Rogers WJ, Yang A, Shapiro EP. Human heart: tagging with MR imaging—a method for noninvasive assessment of myocardial motion. *Radiology*. 1988;169(1):59–63. doi:[10.1148/radiology.169.1.3420283](https://doi.org/10.1148/radiology.169.1.3420283)

2. Bolster BD Jr, McVeigh ER, Zerhouni EA. Myocardial tagging in polar coordinates with use of striped tags. *Radiology*. 1990;177(3):769-772. doi:10.1148/radiology.177.3.2243987
3. Amzulescu MS, De Craene M, Langet H, et al. Myocardial strain imaging: review of general principles, validation, and sources of discrepancies. *Eur Heart J Cardiovasc Imaging*. 2019;20(6):605-619. doi:10.1093/ehjci/jez041
4. Bohs LN, Trahey GE. A novel method for angle independent ultrasonic imaging of blood flow and tissue motion. *IEEE Trans Biomed Eng*. 1991;38(3):280-286. doi:10.1109/10.133210
5. Kaluzynski K, Chen X, Emelianov SY, Skovoroda AR, O'Donnell M. Strain rate imaging using two-dimensional speckle tracking. *IEEE Trans Ultrason Ferroelectr Freq Control*. 2001;48(4):1111-1123. doi:10.1109/58.935730
6. Hor KN, Baumann R, Pedrizzetti G, et al. Magnetic resonance derived myocardial strain assessment using feature tracking. *J Vis Exp*. 2011;48:2356. doi:10.3791/2356
7. Ng A, Swanevelde J. Resolution in ultrasound imaging. *Contin Educ Anaesth Crit Care Pain*. 2011;11(5):186-192. doi:10.1093/bjaceaccp/mkr030
8. Pan L, Stuber M, Kraitchman DL, Fritzsche DL, Gilson WD, Osman NF. Real-time imaging of regional myocardial function using fast-SENC. *Magn Reson Med*. 2006;55(2):386-395. doi:10.1002/mrm.20770
9. Aletras AH, Ding S, Balaban RS, Wen H. DENSE: displacement encoding with stimulated echoes in cardiac functional MRI. *J Magn Reson*. 1999;137(1):247-252. doi:10.1006/jmre.1998.1676
10. Garot J, Bluemke DA, Osman NF, et al. Fast determination of regional myocardial strain fields from tagged cardiac images using harmonic phase MRI. *Circulation*. 2000;101(9):981-988. doi:10.1161/01.CIR.101.9.981
11. Young AA, Axel L, Dougherty L, Bogen DK, Parenteau CS. Validation of tagging with MR imaging to estimate material deformation. *Radiology*. 1993;188(1):101-108. doi:10.1148/radiology.188.1.8511281
12. Arts T, Prinzen FW, Delhaas T, Milles JR, Rossi AC, Clarysse P. Mapping displacement and deformation of the heart with local sine-wave modeling. *IEEE Trans Med Imaging*. 2010;29(5):1114-1123. doi:10.1109/TMI.2009.2037955
13. Ronneberger O, Fischer P, Brox T. U-net: convolutional networks for biomedical image segmentation. In: N Navab, J Hornegger, WM Wells, A Frangi, eds, *International Conference on Medical Image Computing and Computer-Assisted Intervention*. Springer; 2015. doi:10.1007/978-3-319-24574-4\_28
14. Facciolo G, Limare N, Meinhardt-Llopis E. Integral images for block matching. *Image Processing Line*. 2014;4:344-369. doi:10.5201/ipol.2014.57
15. Lewis J. *Fast Normalized Cross-Correlation*. Ind. Light Magic; 2001. 10.
16. Koo TK, Li MY. A guideline of selecting and reporting intraclass correlation coefficients for reliability research. *J Chiropr Med*. 2016;15(2):155-163. doi:10.1016/j.jcm.2016.02.012
17. Wu L, Germans T, Güçlü A, Heymans MW, Allaart CP, van Rossum AC. Feature tracking compared with tissue tagging measurements of segmental strain by cardiovascular magnetic resonance. *J Cardiovasc Magn Reson*. 2014;16(1):10. doi:10.1186/1532-429X-16-10
18. Bucius P, Erley J, Tanacli R, et al. Comparison of feature tracking, fast-SENC, and myocardial tagging for global and segmental left ventricular strain. *ESC Heart Fail*. 2020;7(2):523-532. doi:10.1002/ehf2.12576
19. Backhaus SJ, Metschies G, Zieschang V, et al. Head-to-head comparison of cardiovascular MR feature tracking cine versus acquisition-based deformation strain imaging using myocardial tagging and strain encoding. *Magn Reson Med*. 2021;85(1):357-368. doi:10.1002/mrm.28437
20. Amzulescu M, Langet H, Saloux E, et al. Head-to-head comparison of global and regional two-dimensional speckle tracking strain versus cardiac magnetic resonance tagging in a multicenter validation study. *Circ Cardiovasc Imaging*. 2017;10:e006530. doi:10.1161/CIRCIMAGING.117.006530
21. Militaru S, Panovsky R, Hanet V, et al. Multivendor comparison of global and regional 2D cardiovascular magnetic resonance feature tracking strains vs tissue tagging at 3T. *J Cardiovasc Magn Reson*. 2021;23(1):54. doi:10.1186/s12968-021-00742-3
22. Thomas D, Luetkens J, Faron A, Dabir D, Sprinkart AM, Kuetting D. Feature-tracking-based strain analysis—a comparison of tracking algorithms. *Pol J Radiol*. 2020;85:e97-e103. doi:10.5114/pjr.2020.93610
23. van Everdingen WM, Zweerink A, Nijveldt R, et al. Comparison of strain imaging techniques in CRT candidates: CMR tagging, CMR feature tracking and speckle tracking echocardiography. *Int J Cardiovasc Imaging*. 2018;34(3):443-456. doi:10.1007/s10554-017-1253-5
24. Obokata M, Nagata Y, Wu VC, et al. Direct comparison of cardiac magnetic resonance feature tracking and 2D/3D echocardiography speckle tracking for evaluation of global left ventricular strain. *Eur Heart J Cardiovasc Imaging*. 2016;17(5):525-532. doi:10.1093/ehjci/jev227
25. Pryds K, Larsen AH, Hansen MS, et al. Myocardial strain assessed by feature tracking cardiac magnetic resonance in patients with a variety of cardiovascular diseases—a comparison with echocardiography. *Sci Rep*. 2019;9(1):11296. doi:10.1038/s41598-019-47775-4
26. Ananthapadmanabhan S, Vo G, Nguyen T, Dimitri H, Otton J. Direct comparison of multilayer left ventricular global longitudinal strain using CMR feature tracking and speckle tracking echocardiography. *BMC Cardiovasc Disord*. 2021;21(1):107. doi:10.1186/s12872-021-01916-8
27. Zhong X, Spottiswoode BS, Meyer CH, Kramer CM, Epstein FH. Imaging three-dimensional myocardial mechanics using navigator-gated volumetric spiral cine DENSE MRI. *Magn Reson Med*. 2010;64(4):1089-1097. doi:10.1002/mrm.22503
28. Altiok E, Neizel M, Tiemann S, et al. Quantitative analysis of endocardial and epicardial left ventricular myocardial deformation-comparison of strain-encoded cardiac magnetic resonance imaging with two-dimensional speckle-tracking echocardiography. *J Am Soc Echocardiogr*. 2012;25(11):1179-1188. doi:10.1016/j.echo.2012.07.019
29. ElDeeb SM, Fahmy AS. Accurate harmonic phase tracking of tagged MRI using locally-uniform myocardium displacement constraint. *Med Eng Phys*. 2016;38(11):1305-1313. doi:10.1016/j.medengphy.2016.08.002
30. Cao JJ, Ngai N, Duncanson L, Cheng J, Gliganic K, Chen Q. A comparison of both DENSE and feature tracking techniques with tagging for the cardiovascular magnetic resonance assessment of myocardial strain. *J Cardiovasc Magn Reson*. 2018;20(1):26. doi:10.1186/s12968-018-0448-9
31. Kim D, Gilson WD, Kramer CM, Epstein FH. Myocardial tissue tracking with two-dimensional cine displacement-encoded MR imaging: development and initial evaluation. *Radiology*. 2004;230(3):862-871. doi:10.1148/radiol.2303021213
32. Wang Y, Sun C, Ghadimi S, et al. StrainNet: improved myocardial strain analysis of cine MRI by deep learning from DENSE. *Radiol Cardiothorac Imaging*. 2023;5(3):e220196. doi:10.1148/ryct.220196
33. Auger DA, Ghadimi S, Cai X, et al. Reproducibility of global and segmental myocardial strain using cine DENSE at 3 T: a multicenter cardiovascular magnetic resonance study in healthy subjects and patients with heart disease. *J Cardiovasc Magn Reson*. 2022;24(1):23. doi:10.1186/s12968-022-00851-7
34. Ghadimi S, Auger DA, Feng X, et al. Fully-automated global and segmental strain analysis of DENSE cardiovascular magnetic resonance using deep learning for segmentation and phase unwrapping. *J Cardiovasc Magn Reson*. 2021;23(1):20. doi:10.1186/s12968-021-00712-9



35. Farsalinos KE, Daraban AM, Ünlü S, Thomas JD, Badano LP, Voigt JU. Head-to-head comparison of global longitudinal strain measurements among nine different vendors: the EACVI/ASE inter-vendor comparison study. *J Am Soc Echocardiogr*. 2015;28(10):1171-1181. doi:[10.1016/j.echo.2015.06.011](https://doi.org/10.1016/j.echo.2015.06.011)

**How to cite this article:** Brandt Y, Lubrecht JM, Adriaans BP, et al. Quantification of left ventricular myocardial strain: Comparison between MRI tagging, MRI feature tracking, and ultrasound speckle tracking. *NMR in Biomedicine*. 2024;e5164. doi:[10.1002/nbm.5164](https://doi.org/10.1002/nbm.5164)